CrystEngComm

Continuous Polycrystalline Silicon Layers on Glass grown from Tin Solutions

Journal:	*CrystEngComm*
Manuscript ID	CE-ART-12-2015-002530.R1
Article Type:	Paper
Date Submitted by the Author:	10-Feb-2016
Complete List of Authors:	Bansen, Roman; Leibniz Institute for Crystal Growth Ehlers, Christian; Leibniz Institute for Crystal Growth Teubner, Thomas; Leibniz Institute for Crystal Growth Markurt, Toni; Leibniz Institute for Crystal Growth Schmidtbauer, Jan; Leibniz Institute for Crystal Growth Boeck, Torsten; Leibniz Institute for Crystal Growth,

Journal Name

ARTICLE

Continuous Polycrystalline Silicon Layers on Glass grown from Tin Solutions

Received 00th January 20xx,
Accepted 00th January 20xx

DOI: 10.1039/x0xx00000x

www.rsc.org/

R. Bansen,*[a] C. Ehlers,[a] T. Teubner,[a] T. Markurt,[a] J. Schmidtbauer[a] and T. Boeck[a]

Polycrystalline silicon on glass for photovoltaic applications is grown at low temperatures in a two-step process. In the first step, nanocrystalline Si (nc-Si) films are formed by direct deposition on heated glass substrates at about 400 °C. In the second step, these seed layers serve as templates for the growth of crystalline silicon (c-Si) at temperatures around 600 °C by steady-state solution growth, a process that exhibits significant similarities with float glass production. Using Sn solutions, continuous microcrystalline Si layers with a thickness of about 10 µm are grown. Structural characterization by scanning electron microscopy (SEM) and transmission electron microscopy (TEM) give insights into the growth process of both the seed layer and the thick microcrystalline layer. Chemical characterization by secondary ion mass spectrometry (SIMS) shows low impurity levels, which makes the material interesting for the use in thin-film silicon solar cells.

1. Introduction

Despite the considerable price reductions in Si-based photovoltaics, a large part of the module costs is still based on the high costs of the silicon wafers[1], which is why reducing the solar cell thickness, e.g. by the application of thin-film technologies, remains to be a promising approach in achieving even cheaper, grid-competitive solar cells.[2] The fabrication of Si thin-film solar cells is most often based on the crystallization of an initially amorphous Si film. The silicon is deposited from the vapor phase, e.g by sputtering[3], by physical vapor deposition (PVD),[4] by chemical vapor deposition (CVD),[5] or by deposition from organic solutions.[6] Subsequent crystallization is achieved by an electron beam treatment,[7] by laser irradiation,[8] by thermal annealing in a high temperature furnace,[9] or by the aluminium-induced layer exchange (ALILE) method.[10,11]

Alternatively, crystalline Si can be grown from a metallic solution by liquid phase epitaxy (LPE). Using a low supersaturation during growth, the defect densities in LPE-grown epitaxial layers are lower as compared to e.g. CVD-grown layers. Dislocations arising from the substrate are blocked, carrier diffusion lengths are longer, fewer deep levels occur, and impurities tend to segregate to the liquid rather than the solid.[12,13]

As early as the 1960s and 70s, thin Si films have been deposited on amorphous substrates from metallic solutions.[14,15] In the 1990s, especially the LPE growth of Si layers for PV applications has been investigated. In the growth of polycrystalline Si layers from Sn-Al and Sn-Al-Mg solutions on glass, uniformity and areal density of the crystallites, small grain sizes, or very high growth temperatures remained a problem.[16,17] In other experiments, LPE growth on glass and ceramic substrates from In, Ga and Sn solutions produced high quality Si crystallites, but no coalescent layers.[18–21] The extensive research on the solution growth of c-Si was not able to overcome the limitations, from which common LPE system suffer, though. Especially the narrow temperature process window and the limited amount of dissolved material in the volume of the solvent reservoir constrict the maximum achievable layer thickness. This fundamental shortcoming prevents its application in continuous processes.

We follow a different approach. Crystalline Si is grown epitaxially on seed layers on glass substrates by steady-state liquid phase epitaxy (SSLPE), also known as the temperature difference method (TDM), or steady-state solution growth. Characterized by a continuous delivery of silicon, maintaining the Si supersaturation of the solution in the vicinity of the substrate, SSLPE has no restrictions on the thickness of the deposited layer, it allows for continuous processes, and it can be scaled to almost any size. Essential features of SSLPE are comparable to the float glass process in large-scale industrial glass production. Based on these similarities, there is an opportunity for a successive production of float glass and thin Si films for solar cells in a continuous process in the future.

2. Experimental

In the first process step, a borosilicate glass substrate is heated to about 400 °C from the front side by four halogen lamps in a PVD vacuum chamber. At least 1 µm of Si is deposited on its surface at the same temperature by electron beam

[a] Leibniz Institute for Crystal Growth, Max-Born-Str. 2, 12489 Berlin, Germany.
E-mail: roman.bansen@ikz-berlin.de; Tel: +49 30 6392 3120; Fax: +49 30 6392 3003.
See DOI: 10.1039/x0xx00000x

evaporation (EBE) at deposition rates between 0.5 nm/s and 1 nm/s.

In the second process step, crystalline Si is grown on top of the seed layers by SSLPE. A graphite crucible contains the Sn solution, and a Si feeding source fixed at the bottom. The SSLPE chamber is filled with highly purified hydrogen to prevent oxidation. During growth, a graphite carrier with the sample floats on top of the Sn solution for about 1 h, held in place by a handler arm made from fused silica. Growth temperatures are varied between 550 °C and 700 °C, controlled by graphite heaters at the top, side and bottom of the crucible. A permanent positive temperature difference of a few kelvins between the Si source and the substrate with the seed layer leads to a steady delivery of Si by convective flow through the solvent, and preserves the Si supersaturation in front of the substrate.[22] Before the growth process, a temporary rearrangement of the power of the heaters, leading to a reversed temperature difference, is performed to achieve a slight etching of the seed layer, cf. section 3.2.

SEM characterization of the samples was carried out with a FEI NOVA 600 NanoLab™ dual beam SEM/FIB. Secondary Ion Mass Spectroscopy (SIMS) was performed with a CAMECA IMS 4f and 4fE6 using Cs^+ and O_2^+ as primary ions, respectively.

Transmission electron microscopy (TEM) and high-resolution TEM (HRTEM) characterization were performed with an aberration corrected FEI Titan™ 80-300 operated at 300 kV. Image aberrations were corrected up to the third order by the analysis of Zemlin tableaus,[23] which simultaneously allows to extend the point resolution up to the information limit of the microscope (0.08 nm) and minimize the contrast delocalization (below 0.1 nm).[24] For scanning TEM high-angle annular dark-field (STEM-HAADF) imaging, a semi-convergence angle of 9.0 mrad was used for the electron probe and an inner acceptance semi-angle of 53 mrad for the HAADF detector (Fishione Model 3000). Cross section TEM samples were prepared mechanically by tripod polishing down to a thickness of 15 µm, followed by Ar ion milling with a precision ion polishing system (PIPS™) from Gatan Inc.

3. Results and discussion

3.1 Seed layer.

In the past, direct deposition of Si by CVD at temperatures of about 1130 °C on oxidized Si substrates has been used directly to build solar cells on such material, which led to a maximum solar cell efficiency of 5.0%.[25] In our approach, the material is merely used as a seed layer for the subsequent solution growth process step. When the Si is deposited on the heated glass substrate, the atoms have sufficient energy to move for a certain distance along the surface, before coming to rest. This way, they can find to each other and form small crystalline clusters, leaving a layer of nanocrystalline silicon (nc-Si). No metallic solvents are required, and the process is comparatively swift and easy to handle.

Samples with a thickness of the seed layer of about 1.7 µm were analyzed by TEM. The results are shown in figure 1. It is obvious, that the deposition process does not lead to a homogeneous nanocrystalline layer. Instead, the seed layer is composed of individual 'root-shaped' seed crystals, embedded in a largely amorphous matrix, cf. Fig. 1a. At the surface, the seeds exhibit diameters of several ten to more than 100 nm, cf. Fig. 1b.

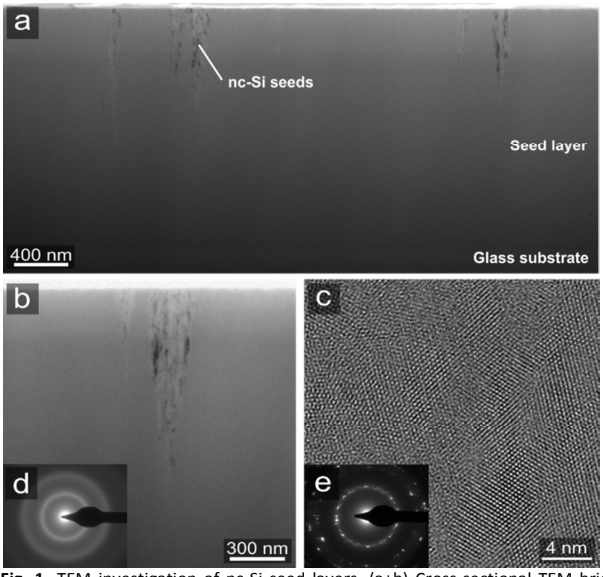

Fig. 1 TEM investigation of nc-Si seed layers. (a+b) Cross-sectional TEM bright field images of seed crystals in a nc-Si seed layer. (c) HRTEM image of a nanocrystalline seed, where several individual grains can be seen. (d+e) SAED images of the seed layer between the seeds (d), and of one of the seeds (e).

Selected area electron diffraction (SAED) patterns of the seed crystals show several individual diffraction spots arranged to Debye-Scherrer rings, which indicates the polycrystalline nature of the seeds, cf. Fig. 1e. High-resolution TEM of the root-shaped crystals reveals grain sizes up to several ten nanometers, cf. Fig. 1c. HRTEM images of the matrix area between the root-shaped seed crystals do not show any lattice fringes and the pattern looks similar to that of amorphous material. In SAED patterns of the Si matrix material multiple strongly blurred Debye-Scherrer rings are visible, indicating the existence of a short range order with very small Si crystallites in all possible orientations, cf. Fig. 1d. The fact that these crystallites are not visible in HRTEM images means they must be smaller than about 1 nanometer. The material can therefore be considered as quasi-amorphous.

In order to determine the areal density of the nanocrystalline seeds on the surface of the seed layer, we analyzed a number of adjacent images with a total lateral field of view of approximately 12.7 µm, manually counting the number of individual nc-Si areas. After determining the average thickness of the TEM specimen in the analyzed region to be about 300 nm, it was possible to approximate the areal density of seeds to be in the range of 1 to 4 seeds/µm².

Based on these TEM results, the seed layer formation is believed to proceed in the following way: the crystallization process starts, when nucleation occurs at some point during PVD growth. A critical nucleus of crystalline Si forms, which eventually extends to a nanocrystal. This process is very similar

to the solid phase crystallization (SPC) of amorphous Si, which has been described in detail by Spinella et al. They found that the nucleation barrier and, as a consequence, the critical radius is temperature independent, amounting to 0.58 nm.[26] All additional Si deposited on top of the nucleus contributes to the growth of the crystallite with a continuous increase in diameter, slowly forming a crystalline cone in the sample – the observed 'root shaped' seeds.

3.2 Oxidation of the seed layer.

A shortcoming of the used growth equipment is the long transfer time of the substrate from the PVD chamber to the SSLPE chamber. Despite handling under high vacuum conditions, the amount of oxygen and water present in the system, at partial pressures of approximately 10^{-7} to 10^{-6} mbar, is sufficiently high to enable the formation of a thin oxide layer on the seed layer's surface during handling and heat-up. This oxide prevents epitaxial growth on the seed crystals in the solution growth step, cf. Fig. 2a+d.

Usually, silicon oxide can easily be removed from Si surfaces by heating the respective substrate up to temperatures of about 900 °C to 1300 °C, depending on the oxide's thickness and surrounding atmosphere.[27,28] However, due to the low softening point of glass, thermal removal of the oxide is impossible.

Therefore we used another approach to overcome the problem of the seed layer oxidation: solution growth was preceded by a short melt-back step. Hereby, the temperature gradient is briefly reversed. This leaves the substrate at the top of the solution in the warmer zone, where the now slightly undersaturated metallic solution starts to dissolve the surface region of the seed layer, and the silicon oxide is, at least partially, removed. The melt-back mode lasts for a period reaching from a few seconds up to two minutes, depending on the general growth temperature and on the applied temperature difference between top and bottom of the solution. Then, the temperature regime is readjusted to the growth mode, and epitaxial growth takes place, cf. Fig. 2e+h.

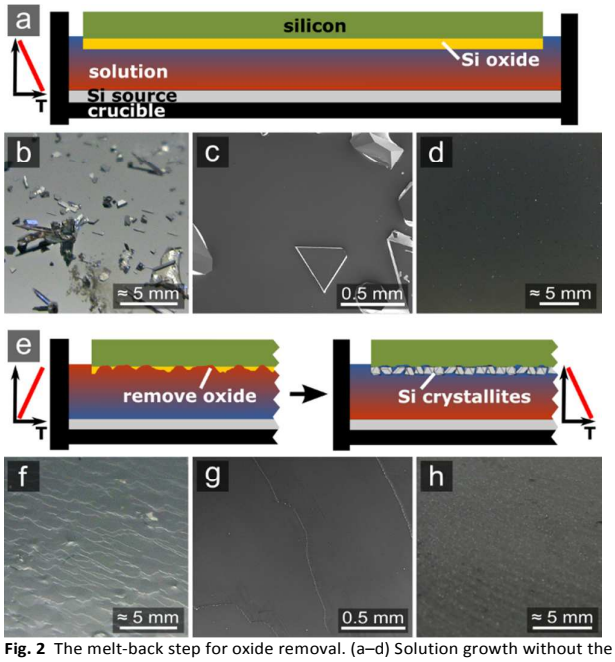

Fig. 2 The melt-back step for oxide removal. (a–d) Solution growth without the melt-back step: the oxide layer hinders epitaxial growth (a), as the photo (b) and SEM micrograph (c) of a Si(111) wafer after growth, as well as the photo of a nc-Si seed layer after growth show (d). (e–h) Using the solution growth step, the oxide layer is removed, allowing for epitaxial growth (e), as can be well seen on the photo (f) and SEM image (g) of exemplary growth on a Si(111) wafer, where step-flow growth leads to a smooth, flat surface, as well as on the photo of Si crystallites grown on a nc-Si seed layer (h).

To verify the functionality of the melt-back procedure in removing the oxide layer and enabling epitaxial growth, we have compared results for growth without and with the melt-back step on oxidized Si(111) substrates. While the duration has to be longer due to the low surface energy of {111} planes, the difference can be observed most easily there. Without a melt-back step, no epitaxial growth takes place and only few isolated crystallites are found on the surface of the oxidized Si(111) substrate (Fig. 2b+c) – similar to the case of growth on nc-Si seed layers, cf. Fig. 2d. In contrast to this, using a melt-back step before switching the temperature regime to the growth mode leads to epitaxial growth on the Si(111) substrate with a smooth surface morphology of the deposited film (Fig. 2f+g).

3.3 SSLPE growth.

3.3.1 SEM characterization. Steady-state solution growth on the nc-Si seed layers with a preceding melt-back step leads to continuous polycrystalline layers, on which all Si crystallites are interconnected. SEM investigations show the large-scale homogeneous coverage of the sample surface with SSLPE-grown silicon crystallites, cf. Fig. 3a. They extend up to 30 µm in diameter, cf. Fig. 3b, and according to SEM cross-sections the average layer thickness amounts to about 10 µm, which is approximately the desired thickness for thin-film Si solar cells.[2,29] The predominant facet orientation of the crystallites is <111>. The areal density of the grains on the surface of the SSLPE-grown layer was determined to be roughly 0.02

grains/µm². It is interesting to note that the inherently rough surface of the as-grown layers can be used for light trapping, which might be beneficial for solar-cell applications.

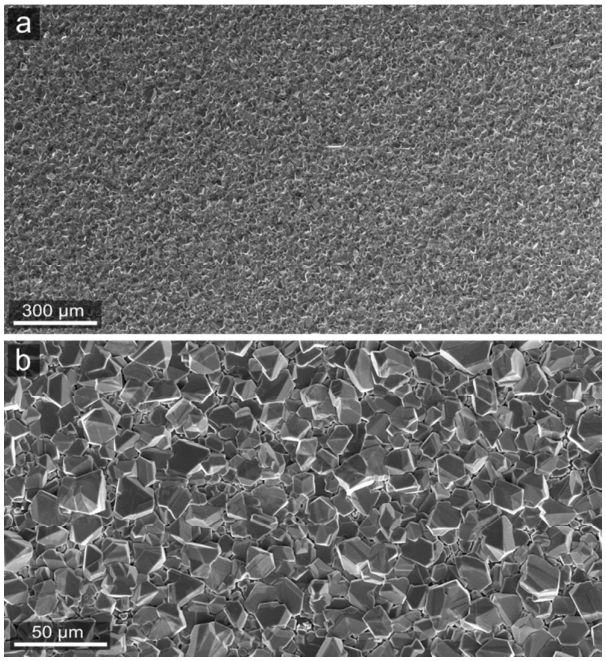

Fig. 3 SEM micrographs of a continuous polycrystalline Si layer, grown by SSLPE from a tin solution on a nc-Si seed layer on glass. (a) Large area overview picture, showing the large scale homogeneity of the layer. (b) More detailed top view showing the individual crystallites forming the layer.

3.3.2 TEM characterization. TEM characterization shows the material grown by SSLPE to be indeed a continuous layer of crystalline material, cf. Fig. 4a+b. The height of this layer varies by several micrometers. The lateral grain size can reach several ten micrometers. While the seed layer is rich in crystal defects, especially dislocations and twin boundaries, the number of defects decreases significantly in the large crystallites on top of the seed layer, which is typical for LPE growth, and has already been observed in the growth from In solutions.[30]

The seed layers were found to have been completely crystallized during the SSLPE process, consisting of large grains that cover several micrometers in diameter, with no amorphous parts left. The grains are penetrated by twin boundaries, reaching all the way from the glass substrate interface deep into the SSLPE-grown crystallites, cf. Fig. 4c+d. This in fact proofs the epitaxial relationship between SSLPE-grown crystallites and grains of the seed layer. While the high crystallinity of the seed layer prevents the attempt to obtain information on where SSLPE growth started and how it evolved, it might be favorable with regard to the intended use of the material in photovoltaics.

The TEM images also show the widespread presence of tin inclusions in the area of the seed layer. Already well visible in the bright field images, their distribution and their significantly more heavy atomic weight than the surrounding material become especially apparent in STEM HAADF micrographs, where they appear much brighter than the silicon or glass, cf. Fig. 4a+b. Also, voids in the seed layer were found along the interface with the glass substrate, which have not been caused by sample preparation.

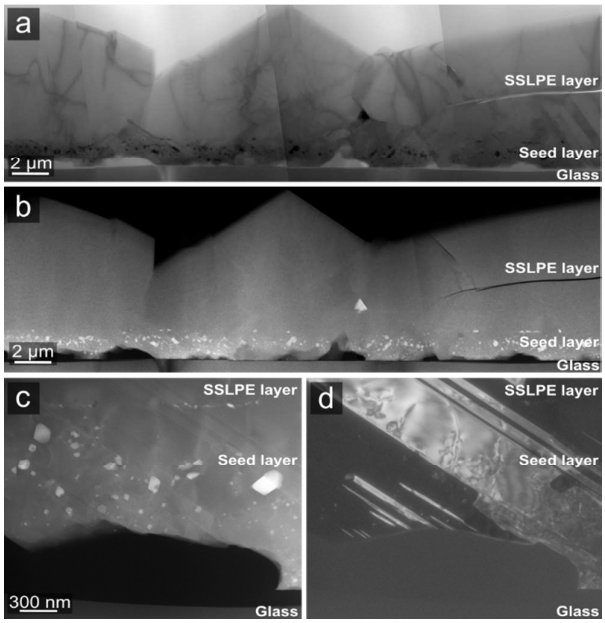

Fig. 4 TEM micrographs of crystallites grown by SSLPE from a tin solution on a nc-Si seed layer on glass. (a+b) Jointed TEM bright field (a) and STEM HAADF (b) overview images, with Sn inclusions appearing in white in the latter. The cracks in the glass substrate and SSLPE layer are preparation-induced. (c+d) Magnification of the seed layer in STEM HAADF mode (c) and TEM dark field mode (d). Twin boundaries prove the crystalline nature of the entire region. Sn inclusions have also accumulated at the seed layer–SSLPE layer interface (c).

As no metallic solvent was used in the seed layer preparation, these large amounts of tin have obviously accumulated during SSLPE growth. This was verified by investigating breaking edges by SEM, where no sample preparation in the form of sawing, polishing or ion milling had taken place.

3.3.3 Interpretation and growth model. The high crystallinity of the seed layers after SSLPE growth is in stark contrast to previous findings from seed layers which were crystallized via the amorphous-liquid-crystalline mechanism before the steady-state solution growth step.[30] The main difference lies in the fact that in the nc-Si seed layers by far most of the volume is still quasi-amorphous at the beginning of SSLPE growth. Amorphous silicon has a higher chemical potential than its crystalline counterpart due to the lower degree of ordering and unsaturated bonds in the volume. Therefore, a-Si has a much higher tendency to dissolve in the Sn solution than c-Si. This leads to the assumption that the large amorphous parts initially present in the seed layer recrystallize below the growing SSLPE crystallites, a process to take place partly from the tin solution directly, and partly by Sn inclusions moving through the amorphous silicon, thereby recrystallizing it. This results in the same orientation of SSLPE crystallites and grains in the seed layer underneath them.

Based on these results, the solution growth process on the nc-Si seed layers is now believed to proceed as follows: Growth

starts by epitaxial enlargement of the root-shaped nanocrystalline seed crystals, cf. Fig. 5a+b.

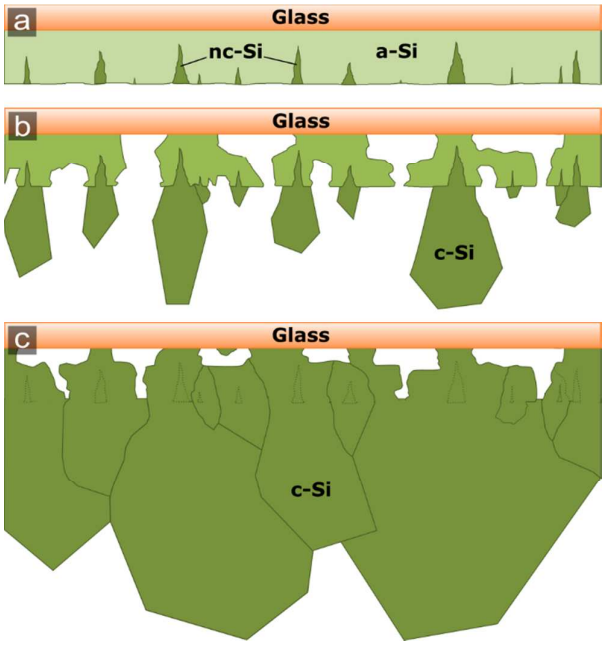

Fig. 5 Schematic depiction of the assumed solution growth process on nc-Si seed layers. The samples are depicted upside down, as SSLPE growth takes place in this way (cf. Fig. 2). (a) Growth starts with a random distribution of seed crystals in the nc-Si seed layer. (b) While epitaxial growth on the seeds leads to the formation of large crystallites, the quasi-amorphous areas partly dissolve in the solution. (c) Eventually, the large crystallites interconnect and the formerly amorphous parts of the seed layer recrystallize in the same orientation as the adjacent crystallites.

Tab. 1 Impurity concentrations of selected elements by SIMS depth profiling of a PVD-grown nc-Si seed layer and a Si layer homoepitaxially grown by SSLPE on a Si wafer from a tin solution, compared with the demands in PV. *The shown value was the measurements' detection limit

Impurity	Concentration in seed layer [atoms/cm^3]	Concentration in SSLPE layer [atoms/cm^3]	PV demand acc. to ref.[32] [atoms/cm^3]	PV demand acc. to ref.[33] [atoms/cm^3]	PV demand acc. to ref.[34] [atoms/cm^3]
Sn	$< 1 \times 10^{16}$ *	6×10^{19}	–	–	–
In	1×10^{17}	$< 1 \times 10^{16}$ *	–	–	–
C	5×10^{17}	3×10^{16}	1.2×10^{17}	1.2×10^{18}	–
O	8×10^{19}	6×10^{16}	1.8×10^{18}	8.8×10^{17}	–
Ti	7×10^{14}	$< 1 \times 10^{14}$ *	1.5×10^{15}	2.9×10^{16}	2.8×10^{16}
Cr	1×10^{16}	$< 1 \times 10^{14}$ *	2.7×10^{16}	2.7×10^{16}	7.8×10^{17}
Fe	7×10^{16}	4×10^{15}	1.3×10^{17}	2.5×10^{17}	2.0×10^{18}
Ni	2×10^{17}	1×10^{16}	2.4×10^{16}	–	–
Cu	6×10^{16}	1×10^{16}	2.2×10^{16}	–	2.2×10^{19}
B	1×10^{15}	$< 7 \times 10^{14}$ *	5.8×10^{16}	1.3×10^{17}	–
Al	8×10^{14}	$< 2 \times 10^{13}$ *	2.6×10^{17}	1.0×10^{17}	7.2×10^{15}

At the same time, the surrounding quasi-amorphous silicon matrix partly dissolves in the solution due to its generally higher solubility, whereby all seed crystals smaller than a critical radius will also dissolve, cf. Fig. 5b. While the crystallites keep growing, the initially amorphous parts of the seed layer are slowly being recrystallized. If the areal density of seed crystals is sufficiently large, the epitaxially grown crystallites on top will interconnect and form a continuous polycrystalline silicon layer eventually, cf. Fig. 5c.

The formation of the gaps along the seed layer–glass interface is believed to be a complex interplay of the filling of dissolved a-Si regions on the one hand, being strongly dependent on the initial areal density of seeds in the nc-Si seed layer, and of the completeness of the oxide layer's removal during the melt-back step on the other hand.

Comparing the areal densities of the grains on the surface of the SSLPE-grown layer (0.02 grains/µm²) with that of the seeds in the subjacent nc-Si seed layer (1 to 4 seeds/µm².), the areal density of large crystallites after solution growth is about two orders of magnitude lower than that of the seeds. The reasons for this difference are primarily the lateral overgrowth of smaller grains, and the dissolution of seeds smaller than the critical grain size. In addition, the accessibility of only those seed crystals, which have been freed from the oxide layer by the melt-back step, is assumed to also play a role.

3.4 SIMS characterization.

Impurity concentrations in both the nc-Si seed layers and the material grown by SSLPE were investigated by SIMS measurements. Thereby, the crystallites grown by SSLPE from a tin solution were consistently too small in size for SIMS investigation. To be still able to measure impurity concentrations, homoepitaxial growth was conducted on a Si(111) wafer at approximately 690 °C to represent the material quality that can be achieved by SSLPE. All other growth parameters and conditions in the growth environment were identical to the usual growth on glass substrates. In table 1, results are shown, and compared to the demands for solar grade (SoG) silicon.

In the seed layer, most impurity concentrations are significantly higher than in the SSLPE layer, whereby most values are still within the required specifications for SoG silicon. The concentrations are remarkably low compared to the results for seed layers formed by the previously applied amorphous-liquid-crystalline (ALC) process.[30,31] If necessary, most of the found impurities in the seed layer could be decreased through a cleaner PVD environment, which has not been a primary concern until now.

For the SSLPE-grown material, the measured impurity levels are very low, considering the fact that no special measures were undertaken to provide an exceptionally clean environment for the growth of the SIMS sample. All impurity concentrations stay well within the specifications for SoG silicon. The most noticeable result is the high impurity level of tin, which can be explained with the silicon-tin phase diagram. The equilibrium concentration of Sn in solid Si around the growth temperature amounts to a mole fraction of 5.7×10^{-4}, about 3×10^{19} atoms/cm³. These high levels of tin in the designated absorber layer are not seen as a problem for the intended use in photovoltaics though. Sn is valence isoelectronic with Si, has neither donor nor acceptor properties in Si, and it is not an effective recombination center.[19,35,36]

4. Conclusions

Seed layers were prepared by direct deposition of Si on heated glass substrates. The advantages of this method lie in the simplicity of the process and in the avoidance of metallic catalysts. TEM characterization of these nc-Si seed layers showed, that they are composed of individual 'root-shaped' crystalline seeds, embedded in a quasi-amorphous matrix.

The seed layers were used as templates for epitaxial enlargement by steady-state liquid phase epitaxy (SSLPE). It was possible to obtain continuous layers, on which the Si crystallites are all interlocked. The layer thickness amounts to about 10 µm, which is approximately the target size for thin-film Si solar cell absorber layers. The high surface roughness has an inherent ability for light trapping.

TEM characterization showed, that the defect density decreases with increasing distance from the seed layer. The seed layer itself shows a high defect density and numerous solvent inclusions. The nanocrystallites have merged into large grains, covering several micrometers in diameter. It was concluded that while epitaxial growth on the seeds leads to the formation of large crystallites, the seed layer's quasi-amorphous parts dissolve in the solution and recrystallize in the same orientation as the adjacent crystallites.

According to SIMS measurements, all impurity concentrations in the SSLPE layer, and most in the seed layer, stay well within the required specifications for solar grade Si. Only tin is incorporated into the material in high amounts, which is not seen as an issue, as Sn is not electrically active in silicon.

Oxidation of the seed layers during handling and heat-up in the HV cluster tool prior to the solution growth step was found to pose an obstacle. A short melt-back step is applied to overcome this issue. Ideally, solution growth would follow the seed layer preparation within a reasonably short time as part of a continuous process, not allowing a sufficiently thick oxide to form.

The main result of this study is the successful growth of continuous Si layers, in which all crystallites are interconnected. The low impurity levels of these layers make them a promising material for the potential use as absorber layers in low-cost thin-film Si solar cells.

Acknowledgements

We want to express our gratitude to Robert Heimburger for ideas and helpful discussions, to RTG Mikroanalyse GmbH Berlin for SIMS measurements, and to Hans-Peter Schramm for ongoing technical assistance.

The conducted research was co-financed by the DFG under contract number BO 1129/5-1.

References

1 D. Van Gestel, I. Gordon and J. Poortmans, *Sol. Energy Mater. Sol. Cells*, 2013, **119**, 261–270.
2 C. Becker, D. Amkreutz, T. Sontheimer, V. Preidel, D. Lockau, J. Haschke, L. Jogschies, C. Klimm, J. J. Merkel, P. Plocica, S. Steffens and B. Rech, *Sol. Energy Mater. Sol. Cells*, 2013, **119**, 112–123.
3 G. Schmidl, G. Andrä, J. Bergmann, A. Gawlik, I. Höger, I. Sill, M. Steglich, F. Falk and G. Mayer, *Mater. Lett.*, 2012, **67**, 229–232.
4 H. Cui, P. R. Campbell and M. a. Green, *Appl. Phys. A*, 2012, **111**, 935–942.

5 R. Buitrago, G. Risso, M. Cutrera, M. Battioni, L. Debernardez, J. Schmidt, R. Arce and R. Koropecki, *Int. J. Hydrogen Energy*, 2008, **33**, 3522–3525.
6 T. Sontheimer, D. Amkreutz, K. Schulz, P. H. Wöbkenberg, C. Guenther, V. Bakumov, J. Erz, C. Mader, S. Traut, F. Ruske, M. Weizman, A. Schnegg, M. Patz, M. Trocha, O. Wunnicke and B. Rech, *Adv. Mater. Interfaces*, 2014, **1**, 1300046.
7 D. Amkreutz, J. Haschke, T. Häring, F. Ruske and B. Rech, *Sol. Energy Mater. Sol. Cells*, 2014, **123**, 13–16.
8 A. Gawlik, J. Plentz, I. Höger, G. Andrä, T. Schmidt, U. Brückner and F. Falk, *Phys. Status Solidi*, 2014, **212**, 162–165.
9 M. A. Green, *Appl. Phys. A*, 2009, **96**, 153–159.
10 O. Nast, T. Puzzer, L. M. Koschier, A. B. Sproul and S. R. Wenham, *Appl. Phys. Lett.*, 1998, **73**, 3214–3216.
11 S. Gall, C. Becker, E. Conrad, P. Dogan, F. Fenske, B. Gorka, K. Y. Lee, B. Rau, F. Ruske and B. Rech, *Sol. Energy Mater. Sol. Cells*, 2009, **93**, 1004–1008.
12 J. B. McNeely, R. B. Hall, A. M. Barnett and W. A. Tiller, *J. Cryst. Growth*, 1984, **70**, 420–426.
13 G. Beaucarne, F. Duerinckx, I. Kuzma, K. Van Nieuwenhuysen, H. J. Kim and J. Poortmans, *Thin Solid Films*, 2006, **511-512**, 533–542.
14 J. D. Filby and S. Nielsen, *J. Electrochem. Soc.*, 1966, **113**, 1091–1092.
15 M. W. M. Graef, L. J. Giling and J. Bloem, *J. Appl. Phys.*, 1977, **48**, 3937.
16 Z. Shi and M. A. Green, *J. Electrochem. Soc.*, 1993, **140**, 3290.
17 Z. Shi, T. L. Young, G. Fu Zheng and M. a. Green, *Sol. Energy Mater. Sol. Cells*, 1993, **31**, 51–60.
18 S. E. A. Schiermeier, C. J. J. Tool, J. A. M. van Roosmalen, L. J. Laas, A. Keitz and W. C. Sinke, in *Proceedings 2nd World Conference on PV Solar Energy Conversion (WCPVSEC)*, Netherlands Energy Research Foundation ECN, Vienna, 1998, pp. 1673–1676.
19 C. J. J. Tool, J. A. M. van Roosmalen, S. E. A. Schiermeier, R. C. Huiberts, G. M. Christie and W. C. Sinke, in *14th European Photovoltaic Solar Energy Conference and Exhibition (EU PVSEC) Proceedings*, Netherlands Energy Research Foundation ECN, Barcelona, 1997, 1–4.
20 J. Kühnle, R. B. Bergmann and J. H. Werner, *J. Cryst. Growth*, 1997, **173**, 62–68.
21 I. Silier, A. Gutjahr, F. Banhart, M. Konuma, E. Bauser, V. Schöllkopf and H. Frey, *Mater. Lett.*, 1996, **28**, 87–91.
22 T. Teubner, R. Heimburger, K. Böttcher, T. Boeck and R. Fornari, *Cryst. Growth Des.*, 2008, **8**, 2484–2488.
23 F. Zemlin, K. Weiss, P. Schiske, W. Kunath and K. Herrmann, *Ultramicroscopy*, 1978, **3**, 49–60.
24 M. Haider, H. Rose, S. Uhlemann, E. Schwan, B. Kabius and K. Urban, *Ultramicroscopy*, 1998, **75**, 53–60.
25 L. Carnel, I. Gordon, D. Van Gestel, G. Beaucarne and J. Poortmans, *Thin Solid Films*, 2008, **516**, 6839–6843.
26 C. Spinella, S. Lombardo and F. Priolo, *J. Appl. Phys.*, 1998, **84**, 5383–5414.
27 F. Abdo, A. Fave, M. Lemiti, A. Pisch and C. Bernard, *Phys. Status Solidi*, 2007, **4**, 1397–1400.
28 F. G. Allen, J. Eisinger, H. D. Hagstrum and J. T. Law, *J. Appl. Phys.*, 1959, **30**, 1563–1571.
29 J. Dore, R. Evans, U. Schubert, B. D. Eggleston, D. Ong, K. Kim, J. Huang, O. Kunz, M. Keevers, R. Egan, S. Varlamov and M. A. Green, *Prog. Photovoltaics Res. Appl.*, 2013, **21**, 1377–1383.
30 R. Bansen, R. Heimburger, J. Schmidtbauer, T. Teubner, T. Markurt, C. Ehlers and T. Boeck, *Appl. Phys. A*, 2015, **119**, 1577–1586.
31 R. Heimburger, N. Deßmann, T. Teubner, H.-P. Schramm, T. Boeck and R. Fornari, *Thin Solid Films*, 2012, **520**, 1784–1788.
32 G. Coletti, D. Macdonald and D. Yang, in *Advanced Silicon Materials for Photovoltaic Applications*, ed. S. Pizzini, John Wiley & Sons, Ltd, Chichester, UK, 2012, 79–125.
33 D. Sarti and R. Einhaus, *Sol. Energy Mater. Sol. Cells*, 2002, **72**, 27–40.
34 B. R. Bathey and M. C. Cretella, *J. Mater. Sci.*, 1982, **17**, 3077–3096.
35 F. A. Trumbore, C. R. Isenberg and E. M. Porbansky, *J. Phys. Chem. Solids*, 1959, **9**, 60–69.
36 P. Capper and M. Mauk, Eds., *Liquid Phase Epitaxy of Electronic, Optical and Optoelectronic Materials*, Wiley, 1st edn., 2007, 114.

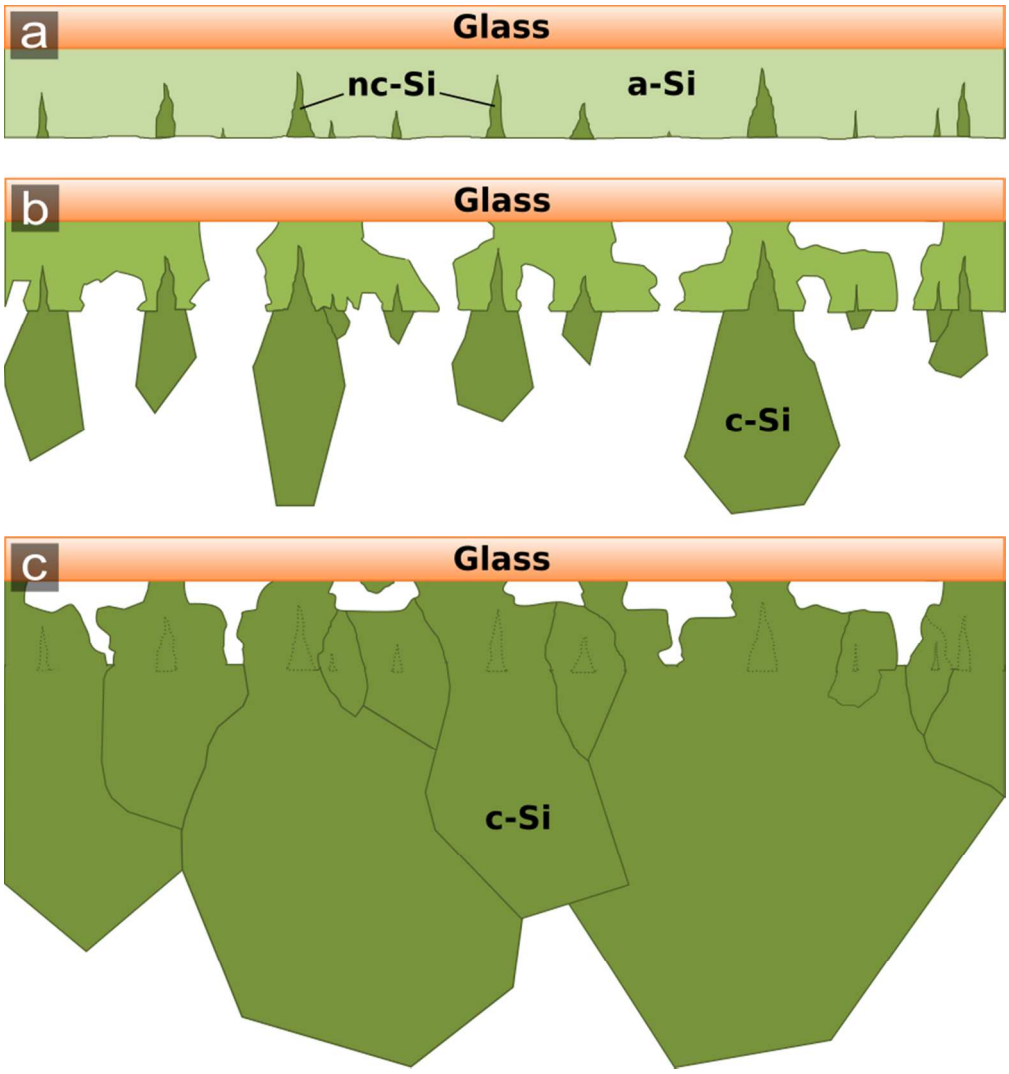
a
Glass
nc-Si
a-Si
b
Glass
c-Si
c
Glass
c-Si